Inorganic Chemistry

pubs.acs.org/IC Article

Negative Thermal Expansion in the Polymorphic Modification of Double Sulfate β-AEu$(SO_4)_2$ (A−Rb^+, Cs^+)

Yuriy G. Denisenko,* Maxim S. Molokeev, Xingxing Jiang, Alexander E. Sedykh, Aleksandr S. Aleksandrovsky, Aleksandr S. Oreshonkov, Evgenii M. Roginskii, Maksim A. Zhernakov, Dominik Heuler, Marcel Seuffert, Zheshuai Lin, Oleg V. Andreev, and Klaus Müller-Buschbaum

Cite This: https://doi.org/10.1021/acs.inorgchem.3c01624 Read Online

ACCESS | Metrics & More | Article Recommendations | Supporting Information

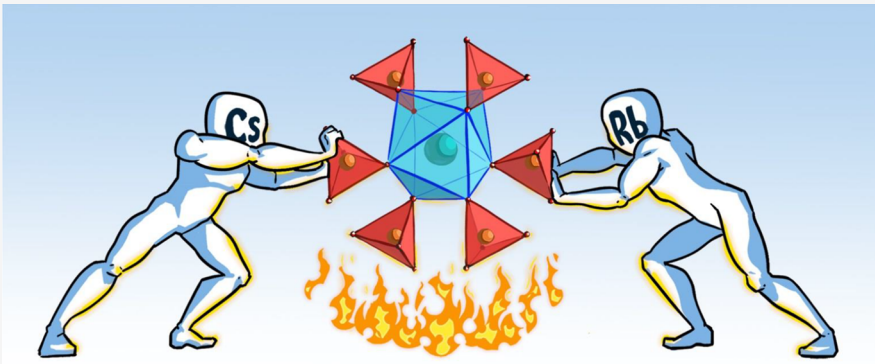

ABSTRACT: New polymorphic modifications of double sulfates β-AEu$(SO_4)_2$ (A−Rb^+, Cs^+) were obtained by the hydrothermal method, the structure of which differs significantly from the monoclinic modifications obtained earlier by solid-state methods. According to single-crystal diffraction data, it was found that the compounds crystallize in the orthorhombic system, space group *Pnna*, with parameters β-RbEu$(SO_4)_2$: a = 9.4667(4) Å, b = 13.0786(5) Å, c = 5.3760(2) Å, V = 665.61(5) Å^3; β-CsEu(SO4)2: a = 9.5278(5) Å, b = 13.8385(7) Å, c = 5.3783(3) Å, V = 709.13(7) Å^3. The asymmetric part of the unit cell contains one-half Rb^+/Cs^+ ion, one-half Eu^{3+} ion, both in special sites, and one SO_4^{2-} ion. Both compounds exhibit nonlinear negative thermal expansion. According to the X-ray structural analysis and theoretical calculations, the polarizing effect of the alkali metal ion has a decisive influence on the demonstration of this phenomenon. Experimental indirect band gaps of β-Rb and β-Cs are 4.05 and 4.11 eV, respectively, while the direct band gaps are 4.48 and 4.54 eV, respectively. The best agreement with theoretical calculations is obtained using the ABINIT package employing PAW pseudopotentials with hybrid PBE0 functional, while norm-conserving pseudopotentials used in the frame of CASTEP code and LCAO approach in the Crystal package gave worse agreement. The properties of alkali ions also significantly affect the luminescent properties of the compounds, which leads to a strong temperature dependence of the intensity of the $^5D_0 \rightarrow {}^7F_4$ transition in β-CsEu$(SO_4)_2$ in contrast to much weaker dependence of this kind in β-RbEu$(SO_4)_2$.

Downloaded via STATE PUBLIC SCITECH LIBRARY SB RAS on August 2, 2023 at 03:05:34 (UTC).
See https://pubs.acs.org/sharingguidelines for options on how to legitimately share published articles.

■ INTRODUCTION

Compounds of rare-earth elements with tetrahedral anions attract researchers' attention as they exhibit many interesting properties.[1−7] In recent years, more and more attention is paid to simple and complex sulfates as functional materials. Among them are phosphors,[8−14] catalysts,[15−21] and gas adsorbents.[22−26] The decisive aspects of the functionalization of rare-earth sulfates are such issues as polymorphism, isomorphism, and crystal-chemical transformations in the technological processes.[27−30]

The vast majority of crystalline compounds undergo expansion in three directions when heated. However, some substances experience zero or negative thermal expansion along one of the directions.[31−39] A significantly smaller number of objects have negative and zero expansion in the entire volume.[40−44] The mechanisms of such behavior are different in all cases and are determined in most cases by coordination effects in the crystal structure.[45−51] Such effects are extremely interesting for creating new highly sensitive materials.[52]

Among the rare earth compounds, crystals carrying Eu^{3+} ions are of particular interest since the ions create effective red

Received: May 17, 2023

 © XXXX American Chemical Society

Table 1. Crystallographic Data and Main Parameters of Processing and Refinement of the Structure of Single Crystals β-AEu$(SO_4)_2$ (A = Rb^+, Cs^+)

single crystals	β-RbEu$(SO_4)_2$		β-CsEu$(SO_4)_2$
M, g/mol	429.56		477.00
Sp. gr., Z		*Pnna*, 2	
T, K		100 (2)	
a, (Å)	9.4667(4)		9.5278(5)
b, (Å)	13.0786(5)		13.8385(7)
c, (Å)	5.3760(2)		5.3783(3)
V, (Å^3)	665.61(5)		709.13(7)
D_x, mg/m^3	4.827		4.468
μ, mm^{-1}	17.322		14.499
		data collection	
wavelength	0.7106 Å (Mo K_α)		0.7106 Å (Mo K_α)
measured reflections	24,683		13,701
independent reflections	2102		1367
reflections with $I > 2\sigma(I)$	1752		954
absorption correction	multiscan		multiscan
R_{int}	0.0709		0.1080
$2\theta_{max}$ (°)	80.56		66.24
h	−17 → 17		−14 → 14
k	−23 → 23		−21 → 21
l	−9 → 9		−8 → 8
		refinement	
number of refined parameters	57		57
$R[F^2 > 2\sigma(F^2)]$	0.0238		0.0357
$wR(F^2)$	0.0573		0.0943
S	1.045		0.799
weight	$w = 1/[\sigma^2(F_o^2) + (0.0254P)^2 ++ 1.426P]$ where $P = \max(F_o^2 + 2F_c^2)/3$		$w = 1/[\sigma^2(F_o^2) ++ (0.1P)^2]$, where, $P = \max(F_o^2 + 2F_c^2)/3$
$(\Delta/\sigma)_{max}$	<0.001		<0.001
largest diff. peak and hole	3.082 and −2.480 e/Å^3		5.055 and −2.617 e/Å^3

photoluminescence, suitable for creating WLED devices with spectral properties similar to daylight. In recent years, the spectroscopic properties of various Eu^{3+}-containing phosphors have been evaluated to see the link between their structural and optical characteristics.[1,2,53−55] However, in the phosphor compounds, the doping level of Eu^{3+} is usually low, and the distribution of Eu^{3+} ions over the corresponding crystallographic positions is often questionable. For this reason, in complex compounds, it is difficult to determine the connection between spectroscopic parameters and the coordination of Eu^{3+} ions in the host lattice. In this situation, europium compounds, in which Eu^{3+} is a constituent element, are more suitable for this purpose since the coordination of Eu^{3+} ions can be accurately determined by the methods of modern crystal structure analysis.[4−7,56−59]

The investigation of the dependencies that govern the band gap of crystalline materials goes back multiple decades. Typically, experimental measurements are supported by DFT calculations and construction of the band structure diagram that allows the determination of the theoretical value of the band gap as the distance between corresponding bands and, consequently, the revealing of the nature of the optical transition governs the onset of the band gap. In modern materials science, numerous computer simulation methods are used, and the choice of methods and approximations plays an important role in the simulation of the properties of specific materials. In some studies, the selection of such tools as certain approximations or functionals is one of the main tasks.[60−64] Unfortunately nowadays, it is rather difficult to predict which set of simulation tools will be the most successful for a specific set of materials.

Previously, it was found that double sulfates AEu$(SO_4)_2$ (A−Rb^+,[65] Cs^+[66]) crystallize in monoclinic modifications. Since we obtained new modifications of these compounds of higher symmetry in this work, we assigned the designation β to them.

RESULTS AND DISCUSSION

Structural Analysis. β-RbEu$(SO_4)_2$ and β-CsEu$(SO_4)_2$ crystallize in the orthorhombic system with the corresponding parameters, which are presented in Table 1. The detailed crystallographic information is shown in Tables S1−S3.

The asymmetric part of the unit cell contains one-half Rb^+/Cs^+ ion (Figure 1), one-half Eu^{3+} ion, and one SO_4^{2-} ion. Eight oxygen atoms from six sulfate groups coordinate each Eu^{3+} ion. Two sulfate groups form a bidentate coordination with the europium(III) ion, the rest monodentate. Thus, each europium(III) ion forms a square antiprism [EuO_8], which is connected to the SO_4^{2-} tetrahedra by nodes and edges, forming two-dimensional Eu$(SO_4)_2$ layers. Rb^+/Cs^+ ions are located between these layers. Each of the [EuO_8] antiprisms binds via the oxygen atoms of the sulfate groups and forms an interesting tetrahedral-antiprismatic junction. Previously, such joints of the "Flügel" type have already been observed in the structures of the rare-earth metal sulfates: β-$Yb_2(SO_4)_3$ and $Y_2(SO_4)_3$.[67]

The analysis of the effect of A^+ cation replacement on either the structural type or the space group has not demonstrated any apparent correlation, as presented in Table S4.[21,30,65,66,68,69] The wide variety of space groups identified for AEu$(SO_4)_2$ compounds suggests a high degree of structural flexibility and variation in the combination of coordination polyhedra. To obtain a more complete data set and to establish any

https://doi.org/10.1021/acs.inorgchem.3c01624
Inorg. Chem. XXXX, XXX, XXX−XXX

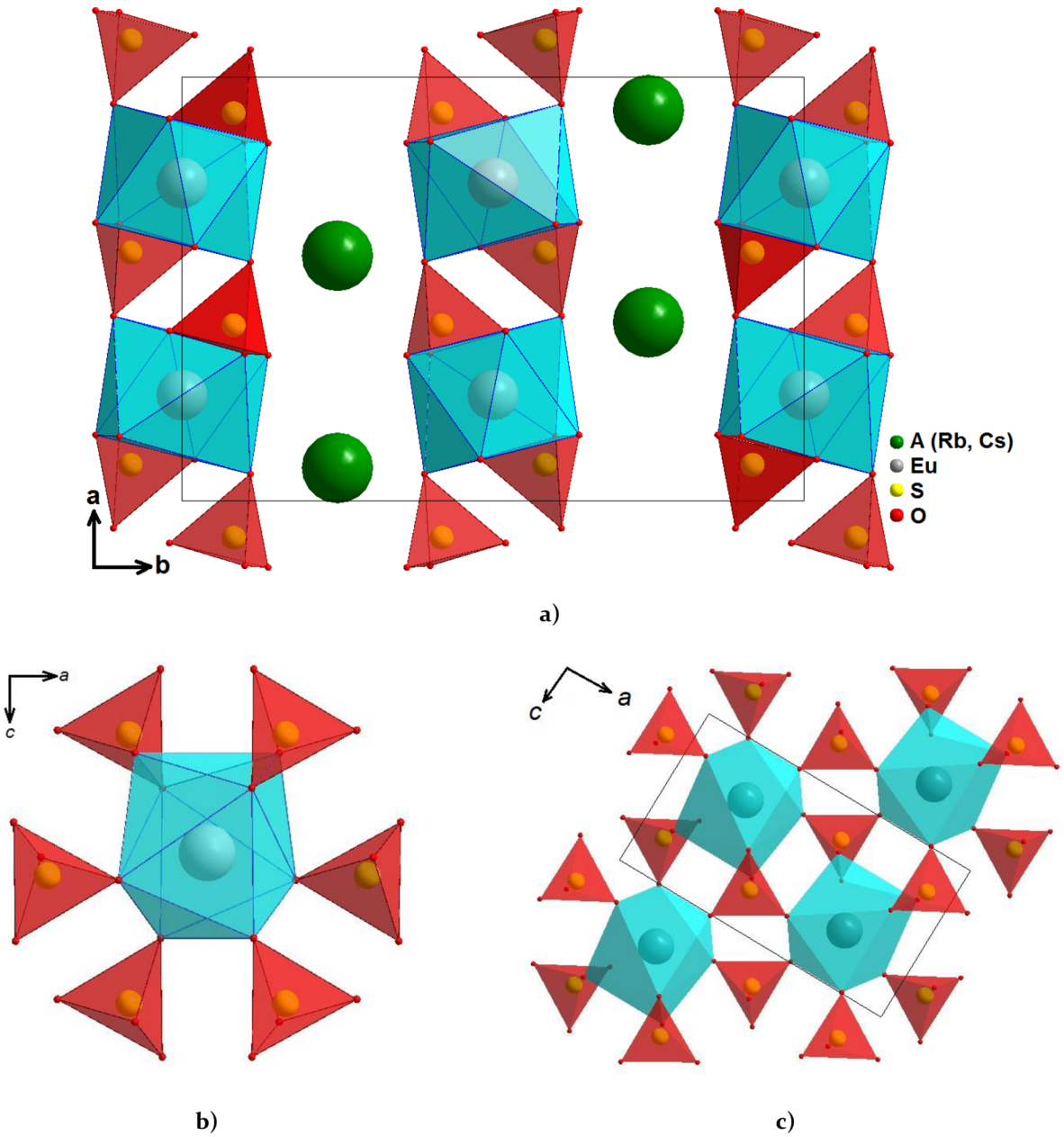

Figure 1. Projections of the crystal structure of β-AEu$(SO_4)_2$ (A = Rb^+, Cs^+) (a), the structure of the tetrahedral-antiprismatic junction {$[EuO_8](SO_4)_6$} of the "Flügel" type (b), and the two-dimensional layers formed by them (c).

dependencies, a more thorough investigation of the structure, including studies of solid solutions, is necessary.

Unit Cell Parameters Thermal Expansion. The cell parameters change under heating of these compounds (Table S4) are depicted in Figure 2. Altogether, the cell parameter trends for either Cs^+ or Rb^+ compounds are similar. Both of them show nonlinear negative thermal expansion of the *a* cell parameter. The *b* cell parameter shows almost identical thermal expansion coefficients 60(2) and 64(2) MK^{-1} for Cs^+ and Rb^+ compounds, respectively, in the range of 300−600 K. The *c* cell parameters and cell volumes also show similar expansion coefficients (Figure 2b,c). Only one significant difference can be marked since the *a* cell parameter and *b* cell parameter in the Cs compound shows about five times bigger module of the thermal parameter in the range of 600−700 K.

The mechanism of the negative expansion in *a* direction seems to be associated with the polarizing effect of the alkali metal in the structure, which displacement, as a result of an increase in the amplitude of thermal vibrations, leads to an increase in the forces of electrostatic attraction between the alkali metal ion and negatively charged oxygen atoms (Figure 3). This interaction leads to a compression of these polyhedra along the *a* direction. To confirm this mechanism, single-crystal X-ray diffraction data of β-RbEu$(SO_4)_2$ were collected at 100 and 300 K. According to the defined crystal structure (see Supporting Information), it can be observed that the interatomic angles along the *a* direction within $[EuO_8]$ polyhedra decreased from 82.93(5) to 82.76(9)° as temperature increases from 100 to 300 K. Although the distances are normally elongated, such decreased angles strongly contribute to the contraction effect, resulting in the net negative thermal expansion along the *a* axis.

https://doi.org/10.1021/acs.inorgchem.3c01624
Inorg. Chem. XXXX, XXX, XXX−XXX

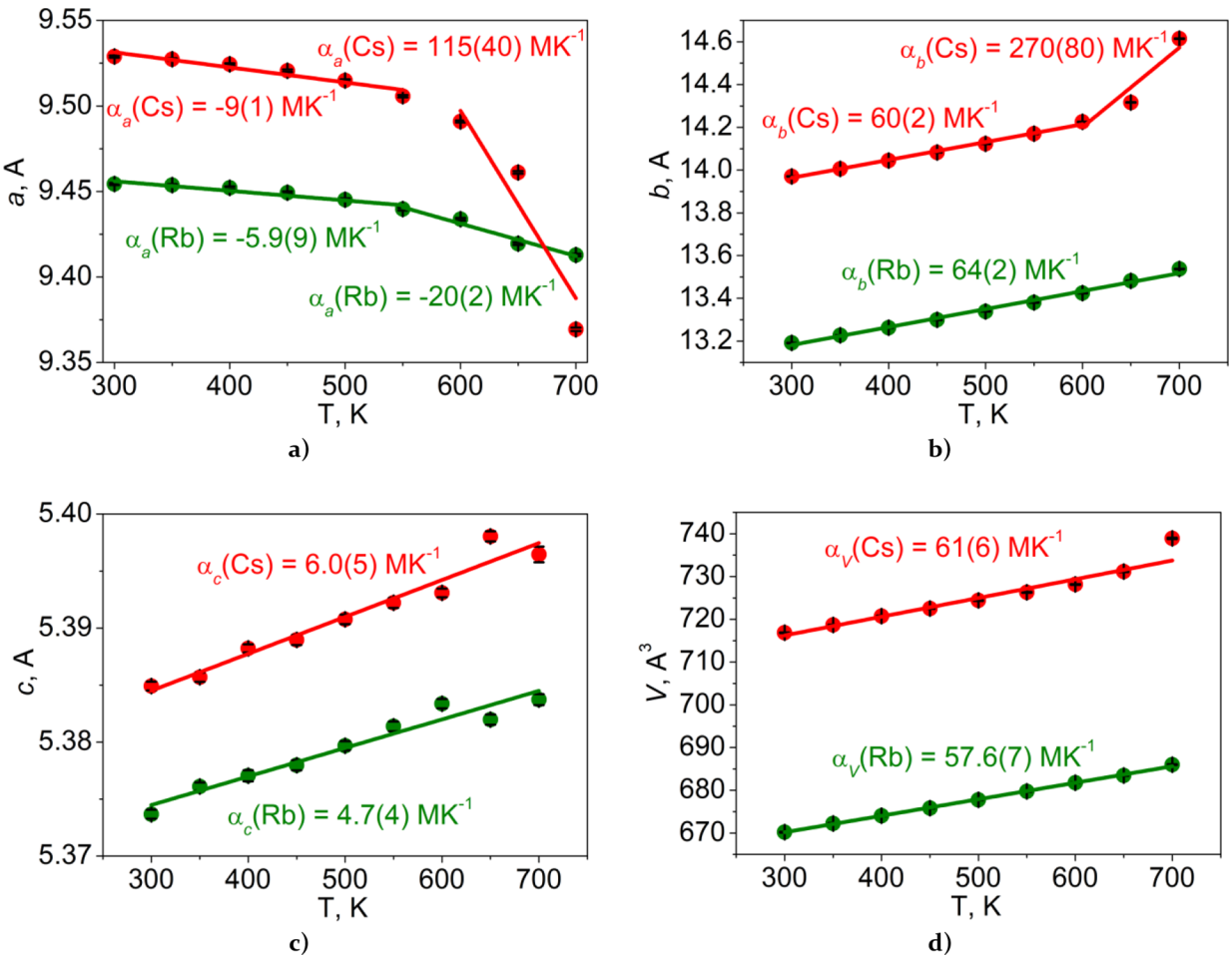

Figure 2. β-AEu$(SO_4)_2$ cell parameter dependence per T: (a) *a* cell parameters; (b) *b* cell parameters; (c) *c* cell parameters; and (d) *V* cell parameters. Thermal expansion coefficients α for all compounds are depicted in the figures.

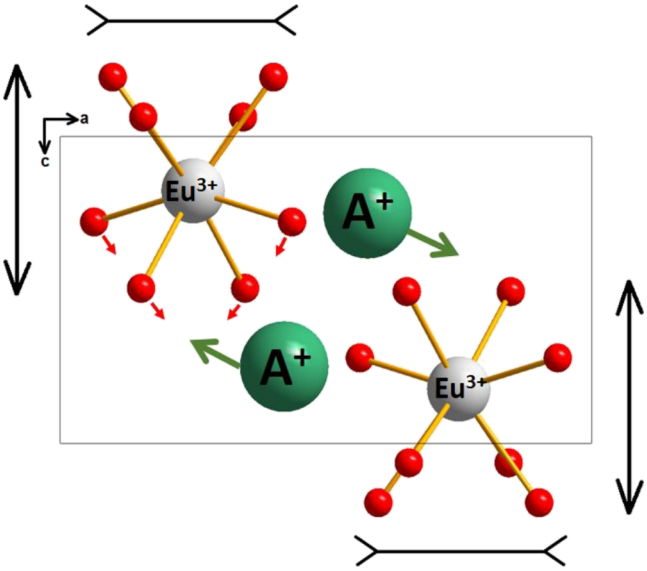

Figure 3. Proposed mechanism of negative thermal expansion in β-AEu$(SO_4)_2$.

To disclose the lattice dynamical mechanism of the negative thermal expansion, here, first-principles phonon simulation was carried out. For the phonon spectrum in both of RbEu$(SO_4)_2$ and CsEu$(SO_4)_2$, none of the imaginary frequencies is observed, confirming the dynamical stability of both compounds. The thermal expansion of a solid is principally due to the anharmonicity of phonons (Figure 4a,b). The Grüneisen parameter, which characterizes the frequency shifting vs lattice volume, is the key to shedding light on the origin of the thermal expansion.

Accordingly, the phonon modes with the negative Grüneisen parameter are positioned at ∼2, 5, 13, and 18THZ for both compounds (Figure 4a,b), suggesting that these modes predominantly contribute to the negative thermal expansion. Atomic vibration assignment reveals that the modes around ∼2THZ originate from the transversal vibration of the interlayer alkali cations (Rb^+ or Cs^+) (Figure 4c), whereas those around ∼5, 13, and 18THZ mainly originate from the distorting vibration of the [EuO_8] polyhedra. This suggests that the anomalous thermal expansion is ascribed to the heat-induced synergetic effect of the transversal vibration of the alkali ion and the distortion vibration of the [EuO_8] polyhedra, which confirms the conclusion deduced from the structural analysis.

Vibrational Spectroscopy. The vibrational (Raman and infrared) spectra of the compounds investigated (Figure 5) are in full agreement with the structural model. Narrow bands in the range from 400 to 500 cm^{-1} related to the symmetric bending $\delta_s(SO_4)$ and bands in the range from 550 to 700 cm^{-1} related to the antisymmetric bending $\delta_{as}(SO_4)$ vibrations of the tetrahedra. Bands in the range from 900 to 1300 cm^{-1} are associated with the stretching of SO_4^{2-} ions. In the Raman spectrum, a strong

https://doi.org/10.1021/acs.inorgchem.3c01624
Inorg. Chem. XXXX, XXX, XXX−XXX

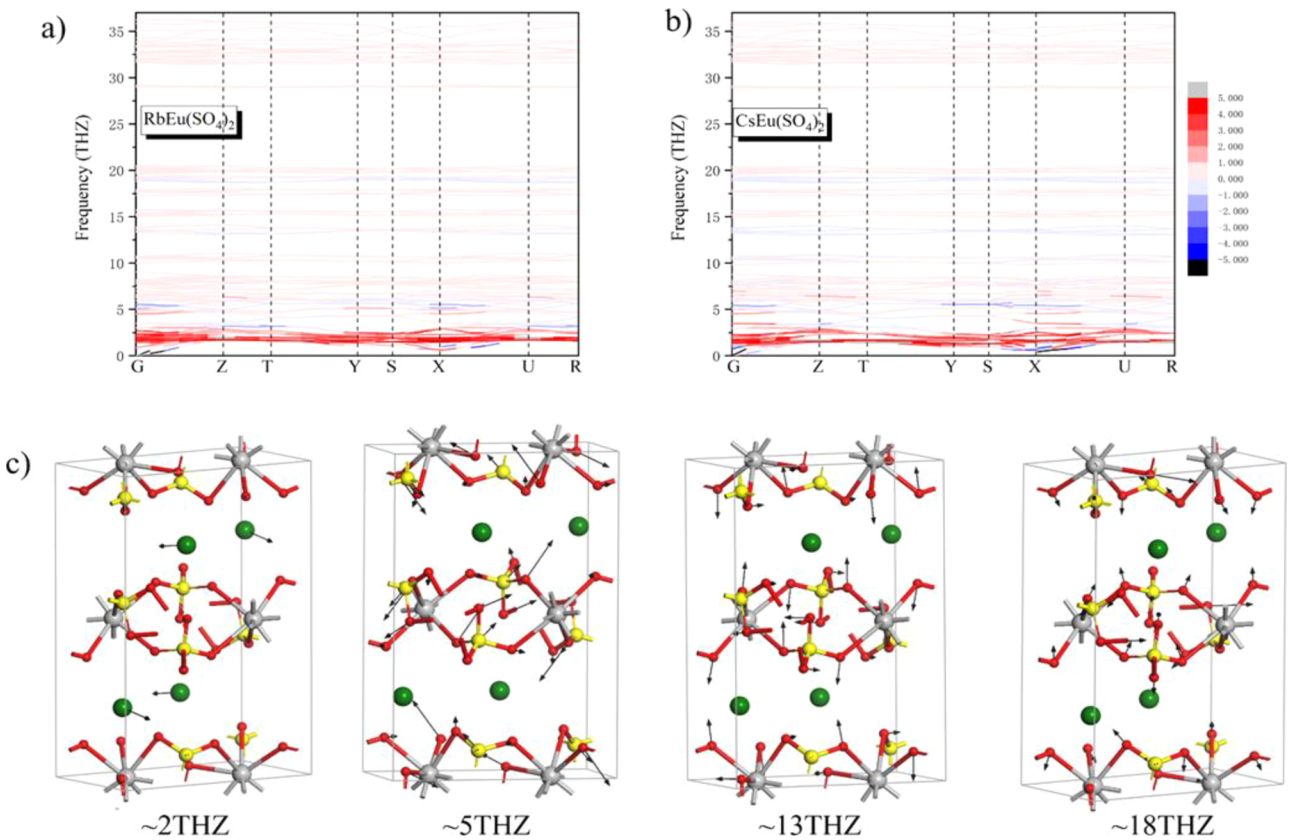

Figure 4. Grüneisen-parameter-weighted phonon spectra of (a) β-RbEu$(SO_4)_2$ and (b) β-CsEu$(SO_4)_2$, and (c) atomic vibration of the phonon modes with negative Grüneisen parameters.

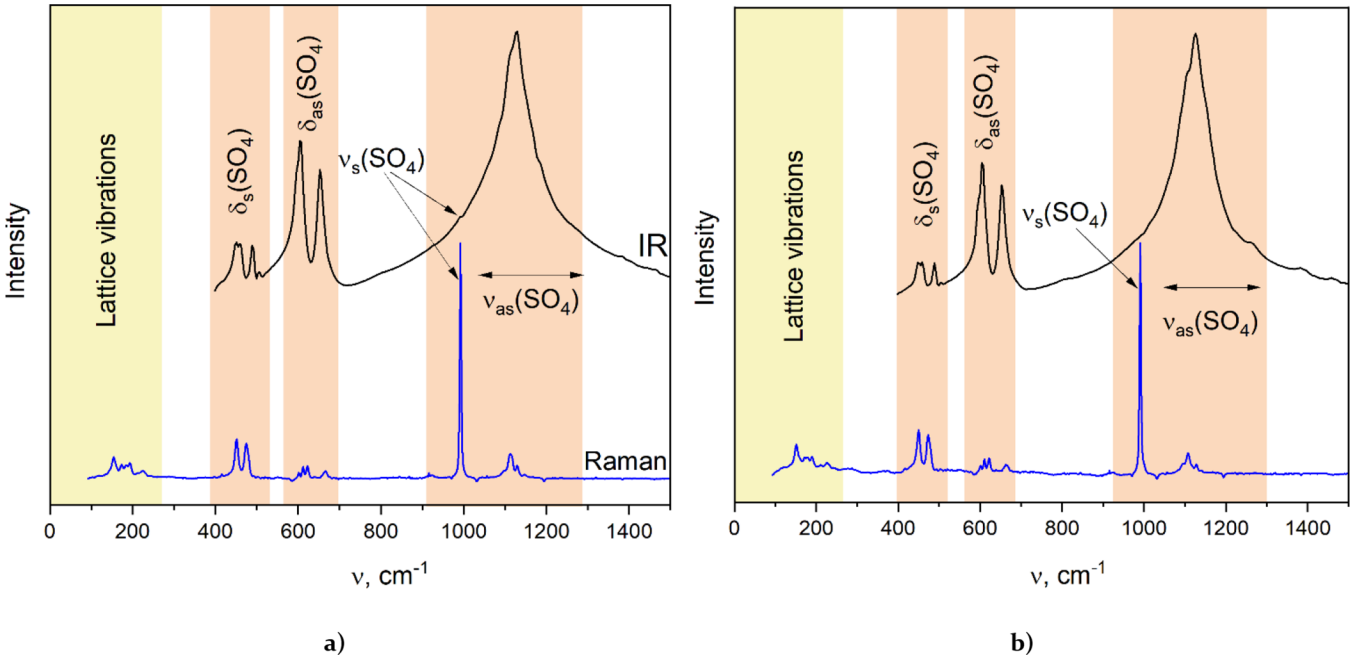

Figure 5. IR (black lines) and Raman (blue lines) spectra of β-AEu$(SO_4)_2$ compounds A = Rb^+ (a) and Cs^+ (b).

narrow band is observed in the region of 1000 cm^{-1} related to the symmetric stretching ($\nu_s(SO_4)$) vibration of the sulfate group, which is practically not observed in the IR spectrum. At the same time, the intensity of the remaining bands associated with antisymmetric stretching $\nu_{as}(SO_4)$ is low in the Raman and high in the IR. The low-intensity bands in the range of low wavenumbers correspond to the lattice modes.

The Brillouin zone (BZ) of the investigated β-sulfates is shown in Figure S1. The chosen path along high symmetry points of the BZ is presented as Γ−X−S−Y−Γ−Z−U−R−T−Z. Coordinates of these points are Γ(0, 0, 0), X(0.5, 0, 0), S(0.5,

https://doi.org/10.1021/acs.inorgchem.3c01624
Inorg. Chem. XXXX, XXX, XXX−XXX

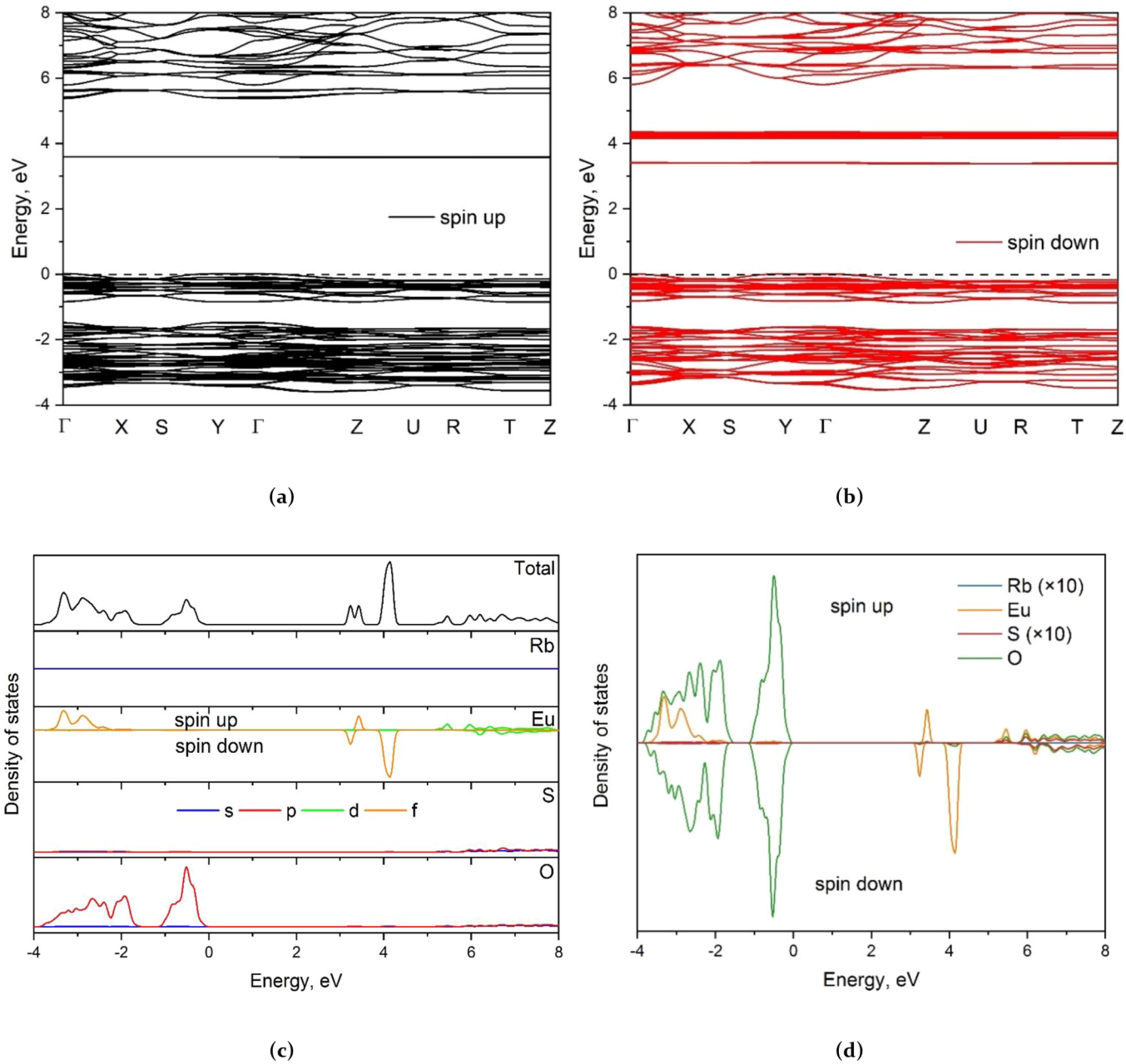

Figure 6. Spin up (a) and spin down (b) electronic structure. Orbital (c) and atom (d) projected density of states for β-RbEu$(SO_4)_2$ calculated in ABINIT code.

0.5, 0), Y(0, 0.5, 0), Z(0, 0, 0.5), U(0.5, 0, 0.5), R(0.5, 0.5, 0.5), T(0, 0.5, 0.5).

Electronic Structure. The electronic structure of the β-RbEu$(SO_4)_2$ calculated by PBE0 is presented in Figure 6. With europium being a lanthanide element, spin-up and spin-down states are shown in different colors (Figure 6a,b). According to this figure, it can be supposed that β-RbEu$(SO_4)_2$ is a dielectric material with E_g equal to 5.42 eV (see Figure 6a). The conduction band minimum (CBM) and valence band maximum (VBM) are located at the Γ point. The CBM is formed by the *d*-electrons of the Eu^{3+} ions, while the VBM is the *p*-electrons of O^{2-} ions (Figure 6c). The narrow flat branches in the range from 3.06 to 4.36 eV in Figure 7a correspond to the localized states between CBM and VBM. According to the analysis of projected densities of states (PDOS) shown in Figure 6c,d, these localized states are revealed as the sharp peak of *f*-orbital electrons in the Eu atom, which can be attributed to unfilled *f*-electron states.

The results of the electronic properties simulations for β-CsEu$(SO_4)_2$ using the PBE0 method are shown in Figure 7. The obtained band gap value (E_g = 5.31 eV) for β-CsEu$(SO_4)_2$ (Figure 7a) is slightly different from the value for β-RbEu$(SO_4)_2$ (Figure 6a). The nature of the electronic transitions in both compounds investigated is the same. Positions of flat *f*-electronic branches slightly shifted from the 2.7 to 4.9 eV range in β-RbEu$(SO_4)_2$ to 2.65−4.85 eV interval in the β-CsEu$(SO_4)_2$.

A comparison of the band gap values obtained using PBE0, LDA + U, meta-GGA + U, and B3LYP approaches is shown in Table 2. The corresponding graphical data can be found in Figures S2 and S3. It should be noted that the difference between LDA + U and meta-GGA + U is only numerical, which is expressed in the difference between the band gap values and

https://doi.org/10.1021/acs.inorgchem.3c01624
Inorg. Chem. XXXX, XXX, XXX−XXX

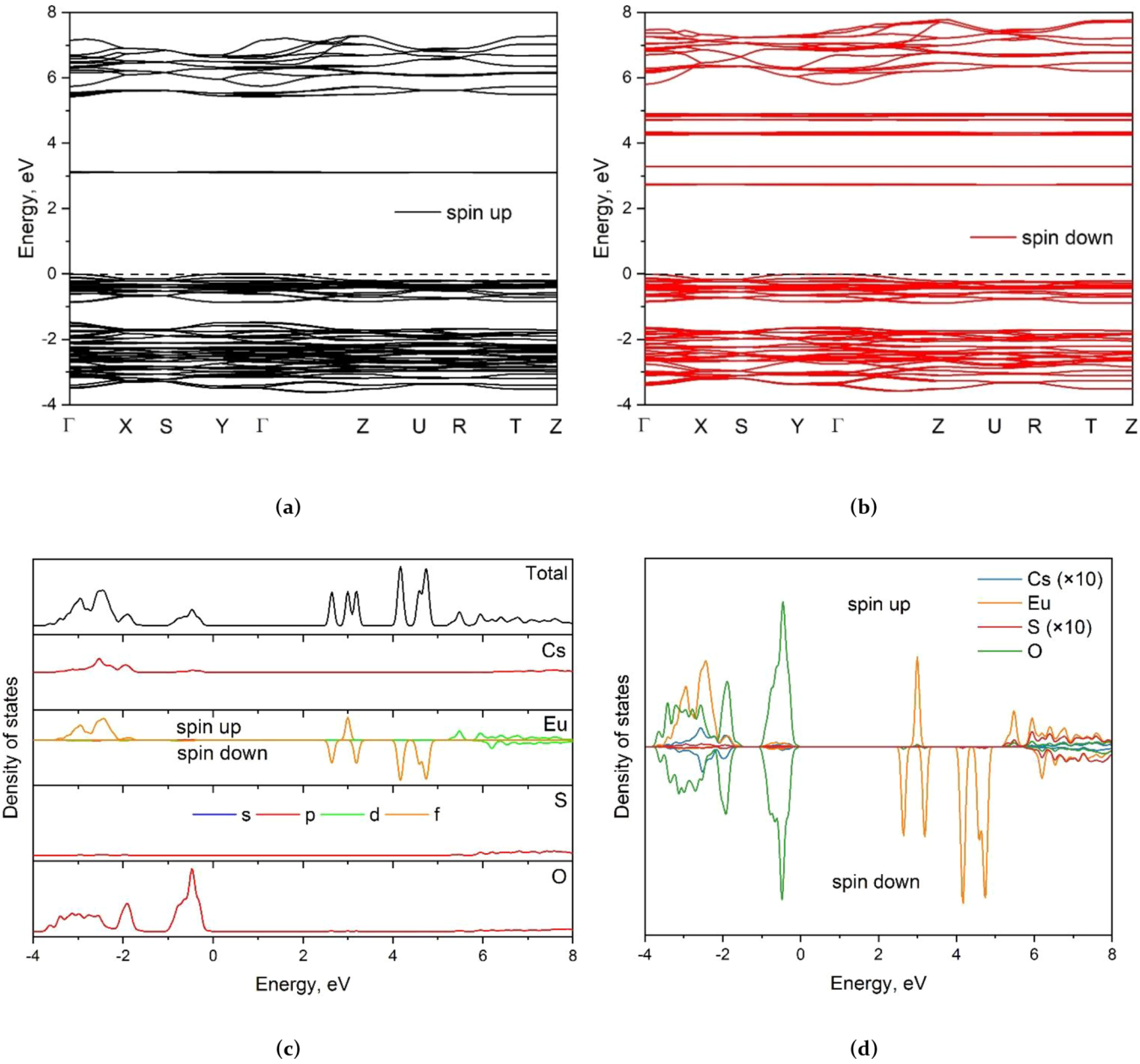

Figure 7. Spin up (a) and spin down (b) electronic structure. Orbital (c) and atom (d) projected density of states for β-$CsEu(SO_4)_2$ calculated in ABINIT code.

Table 2. Calculated Band Gap Values (eV) for the β-$RbEu(SO_4)_2$ and β-$CsEu(SO_4)_2$

compound	PBE0	LDA + U	meta-GGA + U	B3LYP
β-$RbEu(SO_4)_2$	5.42	5.38	5.66	7.09
β-$CsEu(SO_4)_2$	5.31	5.32	5.56	7.09

the position of the localized f-orbital. In the case of β-$RbEu(SO_4)_2$ that flat *f*-electronic branches slightly shifted from 3.4−3.5 to 2.05−2.1 eV and in the case of β-$CsEu(SO_4)_2$ from 3.3−3.4 to 2.0−2.05 eV.

Diffuse reflection spectra of the β-$RbEu(SO_4)_2$ and β-$CsEu(SO_4)_2$ were recorded and used for the determination of optical band gaps. For this purpose, Kubelka−Munk functions modified either for indirect or direct band gap determination were built. Corresponding plots are shown in Figure 8a for indirect bandgaps and in Figure 8b for direct bandgaps. Thus, there is a noticeable difference between the experimental and DFT-calculated values of the direct bandgaps both for β-$RbEu(SO_4)_2$ and β-$CsEu(SO_4)_2$ which is in order of 1 eV.

Luminescence Properties. The most striking feature was observed in the photoluminescence spectra for the corresponding compounds. A strong dependence of the intensity of the $^5D_0 \rightarrow {}^7F_4$ transition on the temperature was observed in the β-$CsEu(SO_4)_2$, while temperature variation of the other radiative transitions is rather traditional and exhibits no peculiarities (Figure 9). Interestingly, the temperature dependence of the $^5D_0 \rightarrow {}^7F_4$ transition is much weaker in the case of β-$RbEu(SO_4)_2$ than in β-$CsEu(SO_4)_2$. To resolve the oddity described above, we can use the Judd−Ofelt parameters Ω_λ, which determine the intensities of individual bands in the spectral regions of *f*−*f* transitions, having distinct origins and appearing variously in different sources. For example, Ω_λ is known to behave differently

https://doi.org/10.1021/acs.inorgchem.3c01624
Inorg. Chem. XXXX, XXX, XXX−XXX

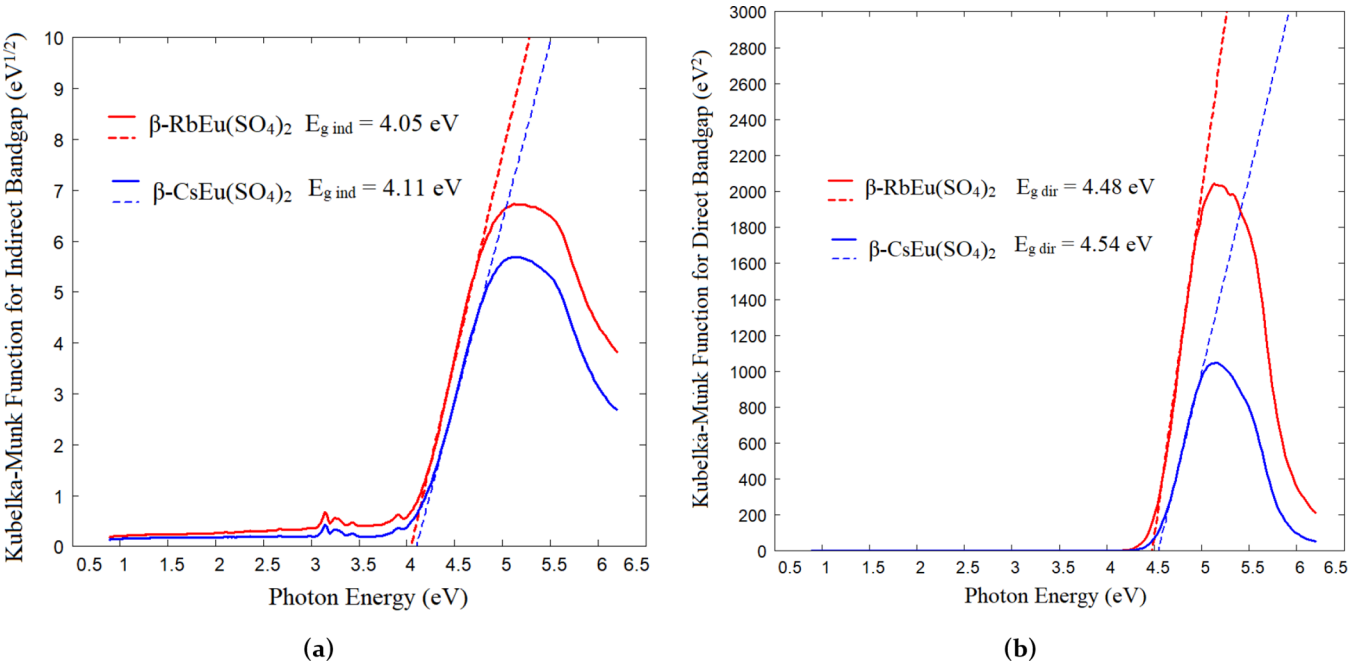

Figure 8. Determination of the indirect (a) and direct (b) band gaps of the corresponding double sulfates.

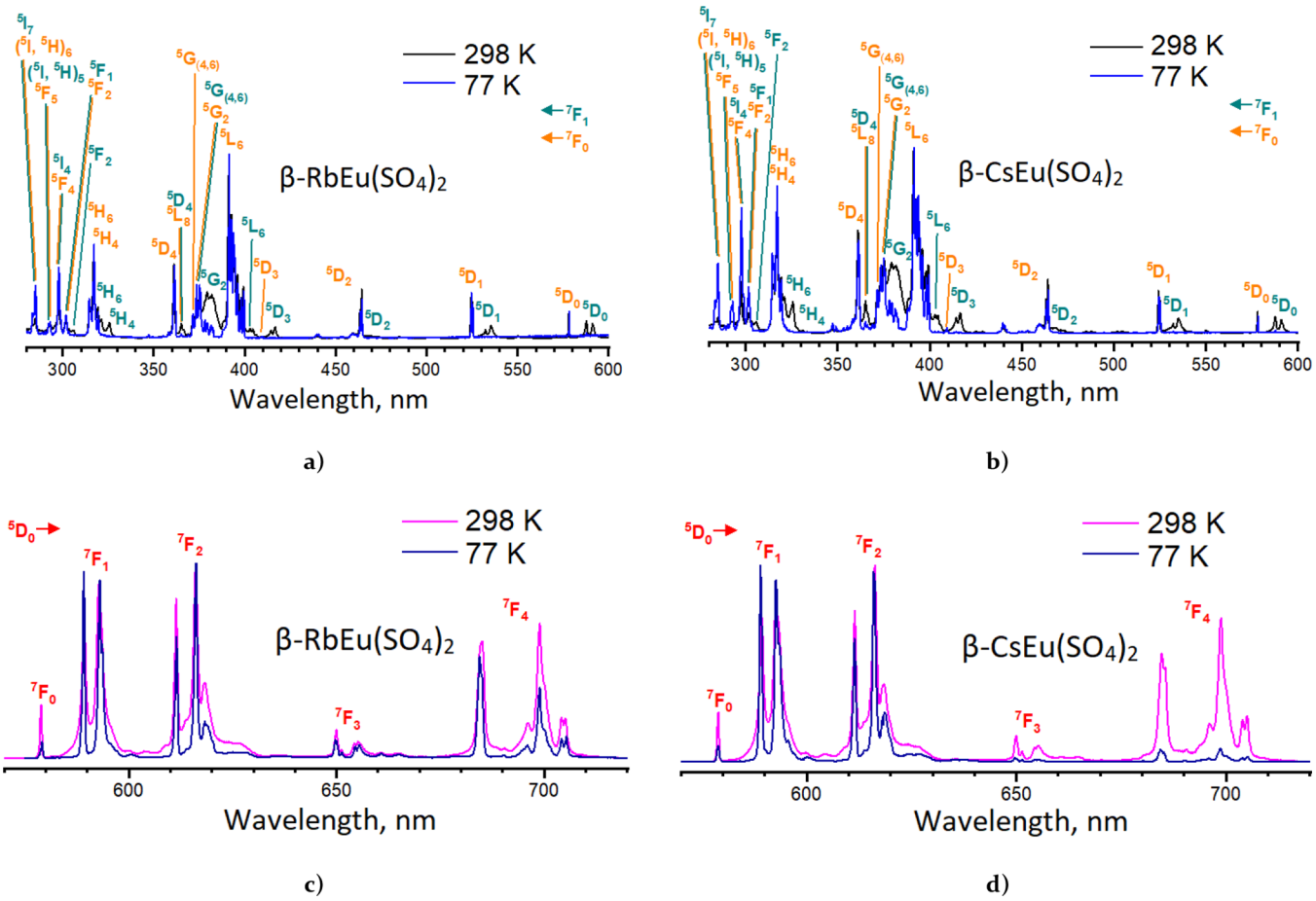

Figure 9. Excitation (a, b) and luminescence (c, d) spectra of β-AEu$(SO_4)_2$ compounds (A^+ = Rb, Cs).

in a system with different polarizability. In 2006, it was shown that in the $Na_9[EuW_{10}O_{36}]\cdot 14H_2O$ compound the Eu^{3+} ions have a slightly distorted D_{4d} local environment and experience an abnormal enhancement of $^5D_0 \rightarrow {}^7F_4$ transition.[70] Recently, we detected a similar effect in the crystal of $AgEu(SO_4)\cdot 2H_2O$ where the local symmetry of Eu^{3+} is C_2.[71] The temperature behavior of the $^5D_0 \rightarrow {}^7F_4$ transition in the β-CsEu$(SO_4)_2$ must be then ascribed to the same effect. In a denser β-RbEu$(SO_4)_2$

https://doi.org/10.1021/acs.inorgchem.3c01624
Inorg. Chem. XXXX, XXX, XXX−XXX

structure, due to the minor variation of the polyhedra, the conditions for observation of that effect become less favorable.

CONCLUSIONS

New polymorphic modifications of double europium(III) sulfates with alkali metals were obtained, and their crystal structure and effects associated with lattice dynamics were systematically studied for the first time. Because of the hydrothermal synthesis, the combination of temperature and pressure leads to the formation of a more compact structure, in contrast to the previously described monoclinic compounds. As shown by high-temperature studies, the compounds experience negative thermal expansion along one of the selected directions at elevated temperatures. By combining X-ray diffraction and theoretical methods, it became possible to determine the role of the polarizing effect of an alkali metal ion in the demonstration of this phenomenon. The presence of highly symmetrical sulfate tetrahedra in the structure determines the high sensitivity of the vibrational properties of the compound. At the same time, the polarizing effect of an alkali ion affects the structure-dependent luminescence properties of the compounds, which leads to a strong temperature dependence of the $^5D_0 \rightarrow {}^7F_4$ transition. Therefore, the compounds obtained are promising highly sensitive functional materials and further studies of this class of compounds are crucial.

ASSOCIATED CONTENT

Supporting Information

The Supporting Information is available free of charge at https://pubs.acs.org/doi/10.1021/acs.inorgchem.3c01624.

Supporting information includes a description of the preparation of the stock solutions, detailed crystallographic data (atomic coordinates, interatomic distances, and thermal expansion parameters), extended images of the electronic structure, calculation and experimental techniques that have been used in this article (PDF)

Accession Codes

CCDC 2252629−2252631 contain the supplementary crystallographic data for this paper. These data can be obtained free of charge via www.ccdc.cam.ac.uk/data_request/cif, or by emailing data_request@ccdc.cam.ac.uk, or by contacting The Cambridge Crystallographic Data Centre, 12 Union Road, Cambridge CB2 1EZ, UK; fax: +44 1223 336033.

AUTHOR INFORMATION

Corresponding Author

Yuriy G. Denisenko − *Institute of Inorganic and Analytical Chemistry, Justus-Liebig-University Gießen, Gießen 35392, Germany; Regional Center "New Generation", Physics and Mathematics School of the Tyumen Region, Tyumen 625051, Russia; Department of Science and Innovation, Tyumen State University, Tyumen 625003, Russia;* orcid.org/0000-0003-3453-5188; Email: yu.g.denisenko@gmail.com

Authors

Maxim S. Molokeev − *Laboratory of Crystal Physics, Kirensky Institute of Physics Federal Research Center KSC SB RAS, Krasnoyarsk 660036, Russia; Department of Engineering Physics and Radioelectronic, Siberian Federal University, Krasnoyarsk 660041, Russia; Department of Physics, Far Eastern State Transport University, Khabarovsk 680021, Russia;* orcid.org/0000-0002-8297-0945

Xingxing Jiang − *Technical Institute of Physics and Chemistry, Chinese Academy of Sciences, Beijing 100190, China;* orcid.org/0000-0001-6068-8773

Alexander E. Sedykh − *Institute of Inorganic and Analytical Chemistry, Justus-Liebig-University Gießen, Gießen 35392, Germany;* orcid.org/0000-0003-2650-5173

Aleksandr S. Aleksandrovsky − *Laboratory of Coherent Optics, Kirensky Institute of Physics Federal Research Center KSC SB RAS, Krasnoyarsk 660036, Russia; Institute of Nanotechnology, Spectroscopy and Quantum Chemistry, Siberian Federal University, Krasnoyarsk 660041, Russia;* orcid.org/0000-0003-1821-6718

Aleksandr S. Oreshonkov − *Laboratory of Molecular Spectroscopy, Kirensky Institute of Physics Federal Research Center KSC SB RAS, Krasnoyarsk 660036, Russia; School of Engineering and Construction, Siberian Federal University, Krasnoyarsk 660041, Russia;* orcid.org/0000-0003-3046-7018

Evgenii M. Roginskii − *Solid State Spectroscopy Department, Ioffe Institute, St. Petersburg 194021, Russia;* orcid.org/0000-0002-5627-5877

Maksim A. Zhernakov − *Institute of Inorganic and Analytical Chemistry, Justus-Liebig-University Gießen, Gießen 35392, Germany; Chemistry Institute, Kazan Federal University, Kazan 420008, Russia*

Dominik Heuler − *Institute of Inorganic and Analytical Chemistry, Justus-Liebig-University Gießen, Gießen 35392, Germany*

Marcel Seuffert − *Institute of Inorganic and Analytical Chemistry, Justus-Liebig-University Gießen, Gießen 35392, Germany*

Zheshuai Lin − *Technical Institute of Physics and Chemistry, Chinese Academy of Sciences, Beijing 100190, China;* orcid.org/0000-0002-9829-9893

Oleg V. Andreev − *Department of Inorganic and Physical Chemistry, Tyumen State University, Tyumen 625003, Russia; Laboratory of the Chemistry of Rare Earth Compounds, Institute of Solid State Chemistry, UB RAS, Yekaterinburg 620137, Russia*

Klaus Müller-Buschbaum − *Institute of Inorganic and Analytical Chemistry, Justus-Liebig-University Gießen, Gießen 35392, Germany; Center for Materials Research (LaMa), Justus-Liebig-University of Giessen, Gießen 35392, Germany*

Complete contact information is available at: https://pubs.acs.org/10.1021/acs.inorgchem.3c01624

Author Contributions

The article was written through contributions of all authors. All authors have given approval to the final version of the article.

Funding

The work was partly carried out within the framework of the Strategic Academic Leadership Program "Priority-2030" for the Siberian Federal University, Tyumen State University, Kazan Federal University and the state assignment of Kirensky Institute of Physics. The calculations were performed in part using facilities of JSCC supercomputer center of RAS.

Notes

The authors declare no competing financial interest.

REFERENCES

(1) Shi, P.; Xia, Z.; Molokeev, M. S.; Atuchin, V. V. Crystal chemistry and luminescence properties of red-emitting $CsGd_{1-x}Eu_x(MoO_4)_2$ solid-solution phosphors. *Dalton Trans.* **2014**, *43*, 9669−9676.

(2) Wang, J.; Luo, L.; Huang, B.; He, J.; Zhang, W.; Zhao, W.; Wang, J. The preparation and optical properties of novel $LiLa(MoO_4)_2:Sm^{3+}$, Eu^{3+} red phosphor. *Materials* **2018**, *11*, 297.

(3) Denisenko, Y. G.; Sedykh, A. E.; Oreshonkov, A. S.; Molokeev, M. S.; Azarapin, N. O.; Sal'nikova, E. I.; Chimitova, O. D.; Andreev, O. V.; Razumkova, I. A.; Müller-Buschbaum, K. Europium (II) Sulfate $EuSO_4$: Synthesis Methods, Crystal and Electronic Structure, Luminescence Properties. *Eur. J. Inorg. Chem.* **2022**, *2022*, No. e202200043.

(4) Abakumov, A. M.; Morozov, V. A.; Tsirlin, A. A.; Verbeeck, J.; Hadermann, J. Cation ordering and flexibility of the BO_4^{2-} tetrahedra in incommensurately modulated $CaEu_2(BO_4)_4$ (B = Mo, W) scheelites. *Inorg. Chem.* **2014**, *53*, 9407−9415.

(5) Ji, H.; Huang, Z.; Xia, Z.; Molokeev, M. S.; Jiang, X.; Lin, Z.; Atuchin, V. V. Comparative investigations of the crystal structure and photoluminescence property of eulytite-type $Ba_3Eu(PO_4)_3$ and $Sr_3Eu(PO_4)_3$. *Dalton Trans.* **2015**, *44*, 7679−7686.

(6) Reshak, A. H.; Alahmed, Z. A.; Bila, J.; Atuchin, V. V.; Bazarov, B. G.; Chimitova, O. D.; Molokeev, M. S.; Prosvirin, I. P.; Yelisseyev, A. P. Exploration of the electronic structure of monoclinic α-$Eu_2(MoO_4)_3$: DFT-based study and X-ray photoelectron spectroscopy. *J. Phys. Chem. C* **2016**, *120*, 10559−10568.

(7) Zhao, D.; Ma, F.-X.; Liu, B.-Z.; Fan, Y.-C.; Han, X.-F.; Zhang, L.; Nie, C.-K. Syntheses, crystal structures and photoluminescence properties of two rare-earth molybdates CsLn(MoO4)2 (Ln = Eu, Tb). *Z. Kristallogr. Cryst. Mater.* **2018**, *233*, 73−79.

(8) Soboleva, L. V.; Pietraszko, A.; Kirpichnikova, L. F.; Shuvalov, L. A. Growth of $Er_2(SO_4)_3 \cdot 8H_2O$ crystals and study of their structure and properties. *Crystallogr. Rep.* **2000**, *45*, 721−722.

(9) Kijima, T.; Shinbori, T.; Sekita, M.; Uota, M.; Sakai, G. Abnormally enhanced Eu^{3+} emission in $Y_2O_2SO_4:Eu^{3+}$ inherited from their precursory dodecylsulfate-templated concentric-layered nanostructure. *J. Lumin.* **2008**, *128*, 311−316.

(10) Kim, S.; Masui, T.; Imanaka, N. Synthesis of Red-emitting Phosphors Based on Gadolinium Oxysulfate by a Flux Method. *Electrochemistry* **2009**, *77*, 611−613.

(11) Kijima, T.; Isayama, T.; Sekita, M.; Uota, M.; Sakai, G. Emission properties of Tb^{3+} in $Y_2O_2SO_4$ derived from their precursory dodecylsulfate-templated concentric- and straight-layered nanostructures. *J. Alloys Compd.* **2009**, *485*, 730−733.

(12) Sharipov, G. L.; Tukhbatullin, A. A.; Abdrakhmanov, A. M. Triboluminescence of crystals and suspensions of inorganic salts of lanthanides. *Prot. Met. Phys. Chem. Surf.* **2011**, *47*, 13−19.

(13) Lian, J. B.; Wang, W. G.; Wang, B. X.; Li, J. Photoluminescence of $(Gd_{1-x}Dy_x)_2O_2SO_4$ Phosphors Synthesized by Homogeneous Precipitation Method. *Adv. Mater. Res.* **2011**, *299−300*, 612−615.

(14) Xing, T. H.; Song, L. X.; Xiong, J.; Cao, H. B.; Du, P. F. Preparation and luminescent properties of Tb^{3+} doped $Y_2O_2SO_4$ microflakes. *Adv. Appl. Ceram.* **2013**, *112*, 455−459.

(15) Flouty, R.; Abi-Aad, E.; Siffert, S.; Aboukaïs, A. Formation of cereous sulphate phase upon interaction of SO_2 with ceria at room temperature. *J. Therm. Anal. Calorim.* **2003**, *73*, 727−734.

(16) Mosaddegh, E.; Asadollah, H. A rapid, one-pot, four-component route to 2H-indazolo [2, 1-b] phthalazine-triones. *Tetrahedron Lett.* **2011**, *52*, 488−490.

(17) Cascales, C.; Lor, B. G.; Puebla, E. G.; Iglesias, M.; Monge, M. A.; Valero, C. R.; Snejko, N. Catalytic Behavior of Rare-Earth Sulfates: Applications in Organic Hydrogenation and Oxidation Reactions. *Chem. Mater.* **2004**, *16*, 4144−4149.

(18) Sohn, J. R.; Lee, S. H.; Lim, J. S. New solid superacid catalyst prepared by doping ZrO_2 with Ce and modifying with sulfate and its catalytic activity for acid catalysis. *Catal. Today* **2006**, *116*, 143−150.

(19) Ikeue, K.; Kawano, T.; Eto, M.; Zhang, D.; Machida, M. X-ray structural study on the different redox behavior of La and Pr oxysulfates/oxysulfides. *J. Alloys Compd.* **2008**, *451*, 338−340.

(20) Mosaddegh, E.; Hassankhani, A. One-pot synthesis of polyhydropyridine derivatives via Hantzsch four component condensation in water medium: Use of a recyclable Lewis acid $[Ce(SO_4)_2 \cdot 4H_2O]$ catalyst. *Bull. Chem. Soc. Ethiop.* **2012**, *26*, 461−465.

(21) Deng, Z.; Bai, F.; Xing, Y.; Xing, N.; Liting, X. Reaction in situ found in the synthesis of a series of lanthanide sulfate complexes and investigation on their structure, spectra and catalytic activity, *Open. J. Inorg. Chem.* **2013**, *03*, 76−99.

(22) Machida, M.; Kawamura, K.; Kawano, T.; Zhang, D.; Ikeue, K. Layered Pr-dodecyl sulfate mesophases as precursors of $Pr_2O_2SO_4$ having a large oxygen-storage capacity. *J. Mater. Chem.* **2006**, *16*, 3084−3090.

(23) Machida, M.; Kawano, T.; Eto, M.; Zhang, D.; Ikeue, K. Ln Dependence of the Large-Capacity Oxygen Storage/Release Property of Ln Oxysulfate/Oxysulfide Systems. *Chem. Mater.* **2007**, *19*, 954−960.

(24) Zhang, D.; Yoshioka, F.; Ikeue, K.; Machida, M. Synthesis and Oxygen Release/Storage Properties of Ce-Substituted La-Oxysulfates, $(La_{1-x}Ce_x)_2O_2SO_4$. *Chem. Mater.* **2008**, *20*, 6697−6703.

(25) Zhang, D.; Kawada, T.; Yoshioka, F.; Machida, M. Oxygen Gateway Effect of $CeO_2/La_2O_2SO_4$ Composite Oxygen Storage Materials. *ACS Omega* **2016**, *1*, 789−798.

(26) Zhang, W.; Arends, I. W. C. E.; Djanashvili, K. Nanoparticles of lanthanide oxysulfate/oxysulfide for improved oxygen storage/release. *Dalton Trans.* **2016**, *45*, 14019−14022.

(27) Atuchin, V. V.; Aleksandrovsky, A. S.; Bazarov, B. G.; Bazarova, J. G.; Chimitova, O. D.; Denisenko, Y. G.; Gavrilova, T. A.; Krylov, A. S.; Maximovskiy, E. A.; Molokeev, M. S.; Oreshonkov, A. S.; Pugachev, A. M.; Surovtsev, N. V. Exploration of structural, vibrational and spectroscopic properties of self-activated orthorhombic double molybdate $RbEu(MoO_4)_2$ with isolated MoO_4 units. *J. Alloys Compd.* **2019**, *785*, 692−697.

(28) Denisenko, Y. G.; Khritokhin, N. A.; Andreev, O. V.; Basova, S. A.; Sal'nikova, E. I.; Polkovnikov, A. A. Thermal decomposition of europium sulfates $Eu_2(SO_4)_3 \cdot 8H_2O$ and $EuSO_4$. *J. Solid State Chem.* **2017**, *255*, 219−224.

(29) Andreev, O. V.; Denisenko, Y. G.; Sal'nikova, E. I.; Khritokhin, N. A.; Zyryanova, K. S. Specifics of reactions of cerium sulfate and europium sulfate with hydrogen. *Russ. J. Inorg. Chem.* **2016**, *61*, 296−301.

(30) Denisenko, Y. G.; Atuchin, V. V.; Molokeev, M. S.; Aleksandrovsky, A. S.; Krylov, A. S.; Oreshonkov, A. S.; Volkova, S. S.; Andreev, O. V. Structure, thermal stability, and spectroscopic properties of triclinic double sulfate $AgEu(SO_4)_2$ with isolated SO4 Groups. *Inorg. Chem.* **2018**, *57*, 13279−13288.

(31) Liu, X.; Wang, J.; Fan, C.; Shang, R.; Cheng, F.; Yuan, B.; Song, W.; Chen, Y.; Liang, E.; Chao, M. Control of Reaction Pathways for Rapid Synthesis of Negative Thermal Expansion Ceramic $Zr_2P_2WO_{12}$ with Uniform Microstructure. *Int. J. Appl. Ceram. Technol.* **2015**, *12*, E28−E33.

(32) Lin, J. C.; Tong, P.; Tong, W.; Lin, S.; Wang, B. S.; Song, W. H.; Zou, Y. M.; Sun, Y. P. Tunable negative thermal expansion related with the gradual evolution of antiferromagnetic ordering in antiperovskite manganese nitrides $Ag_{1-x}NMn_{3+x}$ ($0 \leq x \leq 0.6$). *Appl. Phys. Lett.* **2015**, *106*, No. 082405.

(33) Senn, M. S.; Bombardi, A.; Murray, C. A.; Vecchini, C.; Scherillo, A.; Luo, X.; Cheong, S. W. Negative thermal expansion in hybrid improper ferroelectric Ruddlesden-Popper perovskites by symmetry trapping. *Phys. Rev. Lett.* **2015**, *114*, No. 035701.

(34) Zhao, Y.-Y.; Feng-Xia, H.; Bao, L.-F.; Wang, J.; Hui, W.; Huang, Q.-Z.; Rong-Rong, W.; Liu, Y.; Shen, F.-R.; Kuang, H.; Zhang, M.; Zuo, W.-L.; Zheng, X.-Q.; Sun, J.-R.; Shen, B.-G. Giant negative thermal expansion in bonded MnCoGe-based compounds with Ni_2In-type hexagonal structure. *J. Am. Chem. Soc.* **2015**, *137*, 1746−1749.

(35) Shi, X.-W.; Lian, H.; Qi, R.; Cui, L.; Yao, N. Preparation and properties of negative thermal expansion $Zr_2P_2WO_{12}$ powders and $Zr_2P_2WO_{12}$/TiNi composites. *Mater. Sci. Eng., B* **2016**, *203*, 1−6.

https://doi.org/10.1021/acs.inorgchem.3c01624
Inorg. Chem. XXXX, XXX, XXX−XXX

(36) van Roekeghem, J.; Carrete, N.; Mingo, N. Anomalous thermal conductivity and suppression of negative thermal expansion inScF3. *Phys. Rev. B* **2016**, *94*, No. 020303.
(37) Hu, L.; Chen, J.; Sanson, A.; Wu, H.; Guglieri Rodriguez, C.; Olivi, L.; Ren, Y.; Fan, L.; Deng, J.; Xing, X. New insights into the negative thermal expansion: direct experimental evidence for the "Guitar-String" effect in cubic ScF_3. *J. Am. Chem. Soc.* **2016**, *138*, 8320−8323.
(38) Dangić, Đ.; Murphy, A. R.; Murray, É. D.; Fahy, S.; Savić, I. Coupling between acoustic and soft transverse optical phonons leads to negative thermal expansion of GeTe near the ferroelectric phase transition. *Phys. Rev. B* **2018**, *97*, No. 224106.
(39) Nabetani, K.; Muramatsu, Y.; Oka, K.; Nakano, K.; Hojo, H.; Mizumaki, M.; Agui, A.; Higo, Y.; Hayashi, N.; Takano, M.; Azuma, M. Suppression of temperature hysteresis in negative thermal expansion compound $BiNi_{1-x}Fe_xO_3$ and zero-thermal expansion composite. *Appl. Phys. Lett.* **2015**, *106*, No. 061912.
(40) Barrera, G. D.; Bruno, J. A. O.; Barron, T. H. K.; Allan, N. L. Negative thermal expansion. *J. Phys.: Condens. Matter* **2005**, *17*, R217.
(41) Evans, J. S. O. Negative thermal expansion materials. *J. Chem. Soc., Dalton Trans.* **1999**, *19*, 3317−3326.
(42) Evans, J. S. O.; Mary, T. A.; Sleight, A. W. Negative thermal expansion materials. *Physica B: Condens. Matter.* **1997**, *241−243*, 311−316.
(43) Greve, B. K.; Martin, K. L.; Lee, P. L.; Chupas, P. J.; Chapman, K. W.; Wilkinson, A. P. Pronounced negative thermal expansion from a simple structure: cubic ScF_3. *J. Am. Chem. Soc.* **2010**, *132*, 15496−15498.
(44) Lazar, P.; Bučko, T.; Hafner, J. Negative thermal expansion of ScF_3: Insights from density-functional molecular dynamics in the isothermal-isobaric ensemble. *Phys. Rev. B* **2015**, *92*, No. 224302.
(45) Goodwin, A. L.; Calleja, M.; Conterio, M. J.; Dove, M. T.; Evans, J. S. O.; Keen, D. A.; Peters, L.; Tucker, M. G. Colossal positive and negative thermal expansion in the framework material $Ag_3[Co(CN)_6]$. *Science* **2008**, *319*, 794−797.
(46) Chen, J.; Nittala, K.; Forrester, J. S.; Jones, J. L.; Deng, J.; Ranbo, Y.; Xing, X. The role of spontaneous polarization in the negative thermal expansion of tetragonal $PbTiO_3$-based compounds. *J. Am. Chem. Soc.* **2011**, *133*, 11114−11117.
(47) Huang, R.; Liu, Y.; Fan, W.; Tan, J.; Xiao, F.; Qian, L.; Li, L. Giant negative thermal expansion in $NaZn_{13}$-type $La(Fe,Si,Co)_{13}$ compounds. *J. Am. Chem. Soc.* **2013**, *135*, 11469−11472.
(48) Gava, V.; Martinotto, A. L.; Perottoni, C. A. First-Principles Mode Gruneisen Parameters and Negative Thermal Expansion in α−ZrW_2O_8. *Phys. Rev. Lett.* **2012**, *109*, No. 195503.
(49) Matsuda, T.; Kim, J. E.; Ohoyama, K.; Moritomo, Y. Universal thermal response of the Prussian blue lattice. *Phys. Rev. B* **2009**, *79*, No. 172302.
(50) Köppen, M.; Pankert, D.; Hauptmann, R.; Lang, M.; Weiden, M.; Geibel, C.; Steglich, F. Interference of a first-order transition with the formation of a spin-Peierls state in α'-NaV_2O_5. *Phys. Rev. B* **1998**, *57*, 8466.
(51) Seyidov, M. H. Y.; Suleymanov, R. A. Negative thermal expansion due to negative area compressibility in $TlGaSe_2$ semiconductor with layered crystalline structure. *J. Appl. Phys.* **2010**, *108*, No. 063540.
(52) Jiang, X.; Molokeev, M. S.; Li, W.; Shaofan, W.; Lin, Z.; Yicheng, W.; Chen, C. The mechanism of the area negative thermal expansion in $KBe_2BO_3F_2$ family crystals: A first-principles study. *J. Appl. Phys.* **2016**, *119*, No. 055901.
(53) Tanner, P. A. Some misconceptions concerning the electronic spectra of tri-positive europium and cerium. *Chem. Soc. Rev.* **2013**, *42*, 5090−5101.
(54) Qiao, X.; Seo, H. J. Phase formation and tunable red phosphors of $LiYb_{1-x}Eux(MoO_4)_2$ (x = 0.01-1). *J. Alloys Compd.* **2015**, *648*, 809−817.
(55) Anjie, F.; Guan, A.; Gao, F.; Zhang, X.; Zhou, L.; Meng, Y.; Pan, H. A novel perovskite La_2ZnTiO_6:Eu^{3+} red phosphor for solid state lighting: Synthesis and optimum luminescence. *Opt. Laser Technol.* **2017**, *96*, 43−49.
(56) Chimitova, O. D.; Atuchin, V. V.; Bazarov, B. G.; Molokeev, M. S.; Bazarova, Z. G. The formation and structural parameters of new double molybdates $RbLn(MoO_4)_2$ (Ln = Pr, Nd, Sm, Eu). *Proc. SPIE* **2013**, *8771*, 87711A.
(57) Atuchin, V. V.; Aleksandrovsky, A. S.; Chimitova, O. D.; Gavrilova, T. A.; Krylov, A. S.; Molokeev, M. S.; Oreshonkov, A. S.; Bazarov, B. G.; Bazarova, J. G. Synthesis and spectroscopic properties of monoclinic α-$Eu_2(MoO_4)_3$. *J. Phys. Chem. C* **2014**, *118*, 15404−15411.
(58) Zhao, D.; Ma, F.-X.; Zhi-Qiang, W.; Zhang, L.; Wei, W.; Yang, J.; Zhang, R.-H.; Chen, P.-F.; Shan-Xuan, W. Synthesis, crystal structure and characterizations of a new red phosphor $K_3EuB_6O_{12}$. *Mater. Chem. Phys.* **2016**, *182*, 231−236.
(59) Atuchin, V. V.; Subanakov, A. K.; Aleksandrovsky, A. S.; Bazarov, B. G.; Bazarova, J. G.; Gavrilova, T. A.; Krylov, A. S.; Molokeev, M. S.; Oreshonkov, A. S.; Stefanovich, S. Y. Structural and spectroscopic properties of new noncentrosymmetric self-activated borate $Rb_3EuB_6O_{12}$ with B_5O_{10} units. *Mater. Des.* **2018**, *140*, 488−494.
(60) Borlido, P.; Schmidt, J.; Huran, A. W.; Tran, F.; Marques, M. A. L.; Botti, S. Exchange-correlation functionals for band gaps of solids: benchmark, reparametrization and machine learning. *npj Comput. Mater.* **2020**, *6*, 96.
(61) Castleton, C. W. M.; Lee, A.; Kullgren, J. Benchmarking density functional theory functionals for polarons in oxides: properties of CeO_2. *J. Phys. Chem. C* **2019**, *123*, 5164−5175.
(62) Yang, J. H.; Kitchaev, D. A.; Ceder, G. Rationalizing accurate structure prediction in the meta-GGA SCAN functional. *Phys. Rev. B* **2019**, *100*, No. 035132.
(63) Stahl, B.; Bredow, T. Critical assessment of the DFT + U approach for the prediction of vanadium dioxide properties. *J. Comput. Chem.* **2020**, *41*, 258−265.
(64) Hernández-Haro, N.; Ortega-Castro, J.; Martynov, Y. B.; Nazmitdinov, R. G.; Frontera, A. DFT prediction of band gap in organic-inorganic metal halide perovskites: An exchange-correlation functional benchmark study. *Chem. Phys.* **2019**, *516*, 225−231.
(65) Sarukhanyan, N. L.; Iskhakova, L. D.; Trunov, V. K. Crystal structure of $RbEu(SO_4)_2$. *Kristallografiya* **1983**, *28*, 452−456.
(66) Denisenko, Y. G.; Molokeev, M. S.; Oreshonkov, A. S.; Krylov, A. S.; Aleksandrovsky, A. S.; Azarapin, N. O.; Andreev, O. V.; Razumkova, I. A.; Atuchin, V. V. Crystal Structure, Vibrational, Spectroscopic and Thermochemical Properties of Double Sulfate Crystalline Hydrate $[CsEu(H_2O)_3(SO_4)_2]\cdot H_2O$ and Its Thermal Dehydration Product $CsEu(SO_4)_2$. *Crystals* **2021**, *11*, 1027.
(67) Mills, S. J.; Petříček, V.; Kampf, A. R.; Herbst-Imer, R.; Raudsepp, M. The crystal structure of $Yb_2(SO_4)_3\cdot 3H_2O$ and its decomposition product, β-$Yb_2(SO_4)_3$. *J. Solid State Chem.* **2011**, *184*, 2322−2328.
(68) Sirotinkin, S. P.; Efremov, V. A.; Kovba, L. M.; Pokrovskii, A. N. Crystal structure of lithium-europium double sulfate. *Kristallografiya* **1977**, *22*, 966−970.
(69) Ruiz-Valero, C.; Cascales, C.; Gómez-Lor, B.; Gutiérrez-Puebla, E.; Iglesias, M.; Angeles Monge, A.; Snejko, N. New catalytically active neodymium sulfate. *J. Mater. Chem.* **2002**, *12*, 3073−3077.
(70) Sá Ferreira, R. A.; Nobre, S. S.; Granadeiro, C. M.; Nogueira, H. I. S.; Carlos, L. D.; Malta, O. L. A Theoretical Interpretation of the Abnormal $^5D_0 \rightarrow {}^7F_4$ Intensity Based on the Eu^{3+} Local Coordination in the $Na_9[EuW_{10}O_{36}]\cdot 14H_2O$ Polyoxometalate. *J. Lumin.* **2006**, *121*, 561−567.
(71) Denisenko, Y. G.; Sedykh, A. E.; Molokeev, M. S.; Oreshonkov, A. S.; Aleksandrovsky, A. S.; Krylov, A. S.; Khritokhin, N. A.; Sal'nikova, E. I.; Andreev, O. V.; Müller-Buschbaum, K. Crystal and electronic structure, thermochemical and photophysical properties of europium-silver sulfate monohydrate $AgEu(SO_4)_2\cdot H_2O$. *J. Solid. State Chem.* **2021**, *294*, No. 121898.

https://doi.org/10.1021/acs.inorgchem.3c01624
Inorg. Chem. XXXX, XXX, XXX−XXX